Supplement of

Influence of irradiance and mixing layer height on the vertical trace matter distribution in the lower planetary boundary layer – drone-based investigation

Lasse Moormann[1], Friederike Fachinger[1], Holger Tost[2], Frank Drewnick[1]

[1] Multiphase Chemistry Department, Max Planck Institute for Chemistry, Mainz, 55128, Germany
[2] Institute for Atmospheric Physics, Johannes Gutenberg University, Mainz, 55128, Germany

Correspondence to: Frank Drewnick (frank.drewnick@mpic.de)

S1: Tables

Table S1: Instruments used for characterization of the lower troposphere.

Instrument	Measured variables	Time resolution
	MoLa (Drewnick et al., 2012)	
CPC[a]	Particle number concentration (> 2.5 nm)	1 s
EDM[b]	Particulate matter PM_1	6 s
FMPS[c]	Particle size distribution (5.6 to 560 nm) based on electrical mobility diameter	1 s
Meteorological station[d]	Wind direction, wind speed, relative humidity, temperature, rain intensity, pressure	1 s
OPC[e]	Particle size distribution (0.25 to 32 µm) based on optical diameter	6 s
O_3-monitor[f]	Mixing ratio of O_3	2 s
Pyranometer[g]	Solar irradiance	1s
[a]Condensation Particle Counter Model 3786, TSI, Inc., USA. [b]Environmental Dust Monitor EDM180, Grimm Aerosoltechnik, Germany. [c]Fast Mobility Particle Sizer Model 3091, TSI, Inc., USA. [d]WXT520, Vaisala Oyj, Finland. [e]Optical Particle Counter Model 1.109, Grimm Aerosoltechnik GmbH, Germany. [f]Monitor 205 Dual Beam Ozone Monitor, 2B Technologies, Inc., USA. [g]CMP3 Pyranometer Sensor, Campbell Scientific Inc., UK.		
	FLab (Moormann et al., 2025)	
Anemometer[h]	Horizontal wind speed and direction; temperature; relative humidity; pressure	1 s
CPC[i]	Particle number concentration (> 10 nm)	1 s
CBO[j]	Mixing ratio of CO_2	2 s
OPC[k]	Particle size distribution (0.350 to 40 µm) based on optical diameter; temperature; relative humidity	1 s
O_3-monitor[l]	Mixing ratio of O_3	2 s
UAS: Matrice 600[m]	3D orientation; 3D flight velocity; GPS position; wind speed and direction; altitude based on pressure level and GPS; propeller rotation rate; various internal data	≤1 s
[h]TriSonica™ Mini, Anemoment LLC, USA. [i]Condensation Particle Counter Model 3007, TSI, Inc., USA. [j]CARBOCAP® Carbon Dioxide Probe GMP343, Vaisala Ojy, Finland. [k]OPC-N3, Alphasense AMETEK®, United Kingdom. [l]Model 205 Dual Beam Ozone Monitor, 2B Technologies, Inc., USA. [m]Matrice 600, SZ DJI Technology Co., Ltd., China.		
	Flux tower	
Ultra-sonic anemometer[n]	3D wind direction, humidity, temperature	0.05 s
[n]CSAT3B 3-D Sonic Anemometer, Campbell Scientific, Inc., Logan, Utah, USA.		

S2: Figures

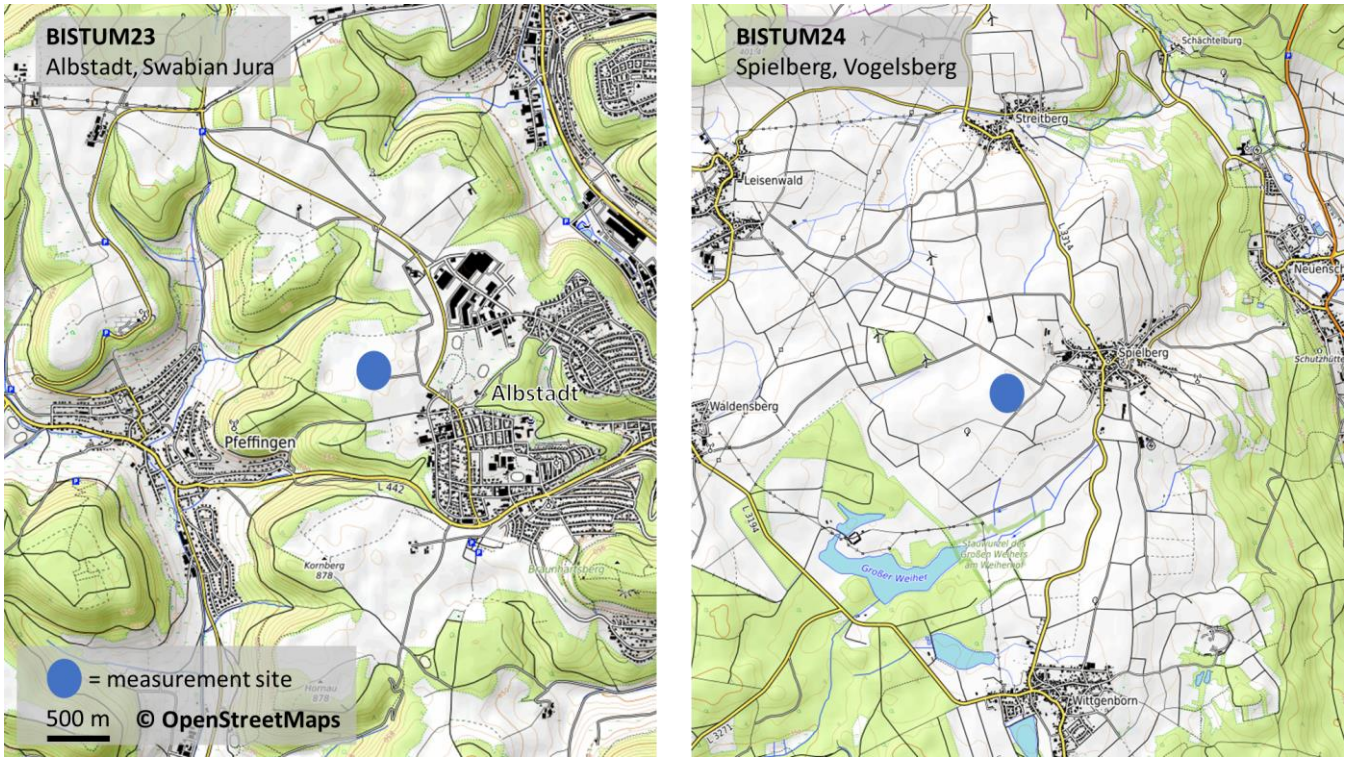

Figure S1: Topographic maps of the rural measurement sites during BISTUM23 and BISTUM24.

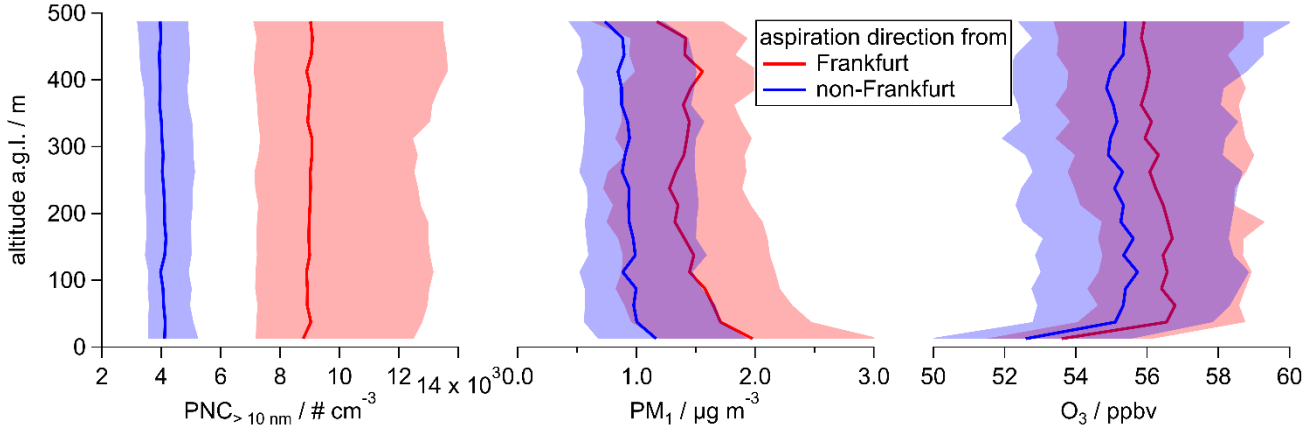

Figure S2: Median vertical profiles of anthropogenic tracers for air masses passing the Frankfurt-Rhine-Main metropolitan area (red) and only rural areas (blue): during BISTUM24 the particle number concentration (a), the PM_1 mass concentration (b) and O_3 mixing ratio (c). Shaded areas represent the respective interquartile ranges.

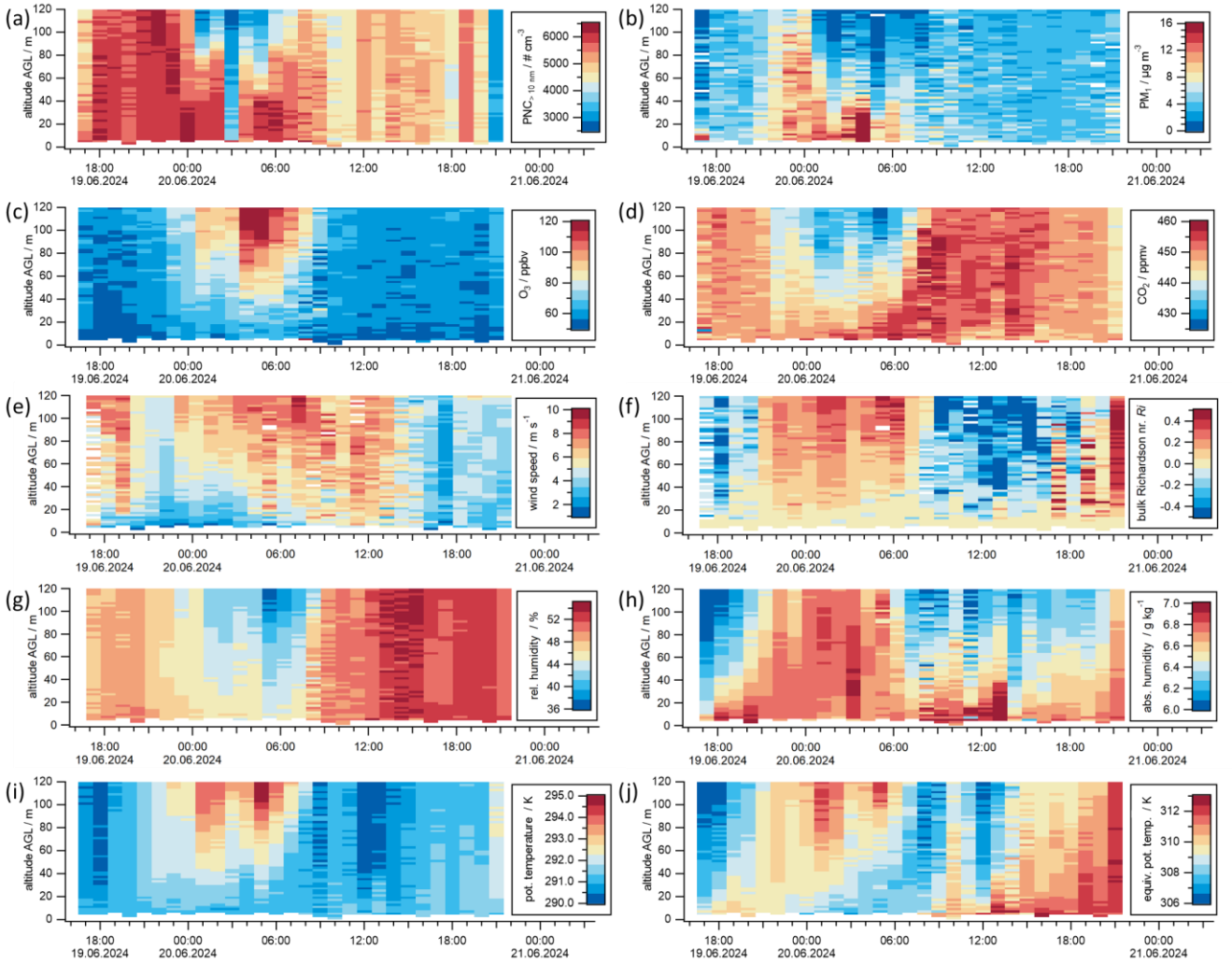

Figure S3: Hourly high-resolution (2 m bins) vertical profiles throughout a full day and night during BISTUM24, including: the particle number concentration measured with the CPC ($PNC_{>10\ nm}$) (a), PM_1 (b), O_3 (c), CO_2 (d), wind speed (e), bulk Richardson number (f), relative and absolute humidity (g and h), and potential and equivalent potential temperature (i and j).

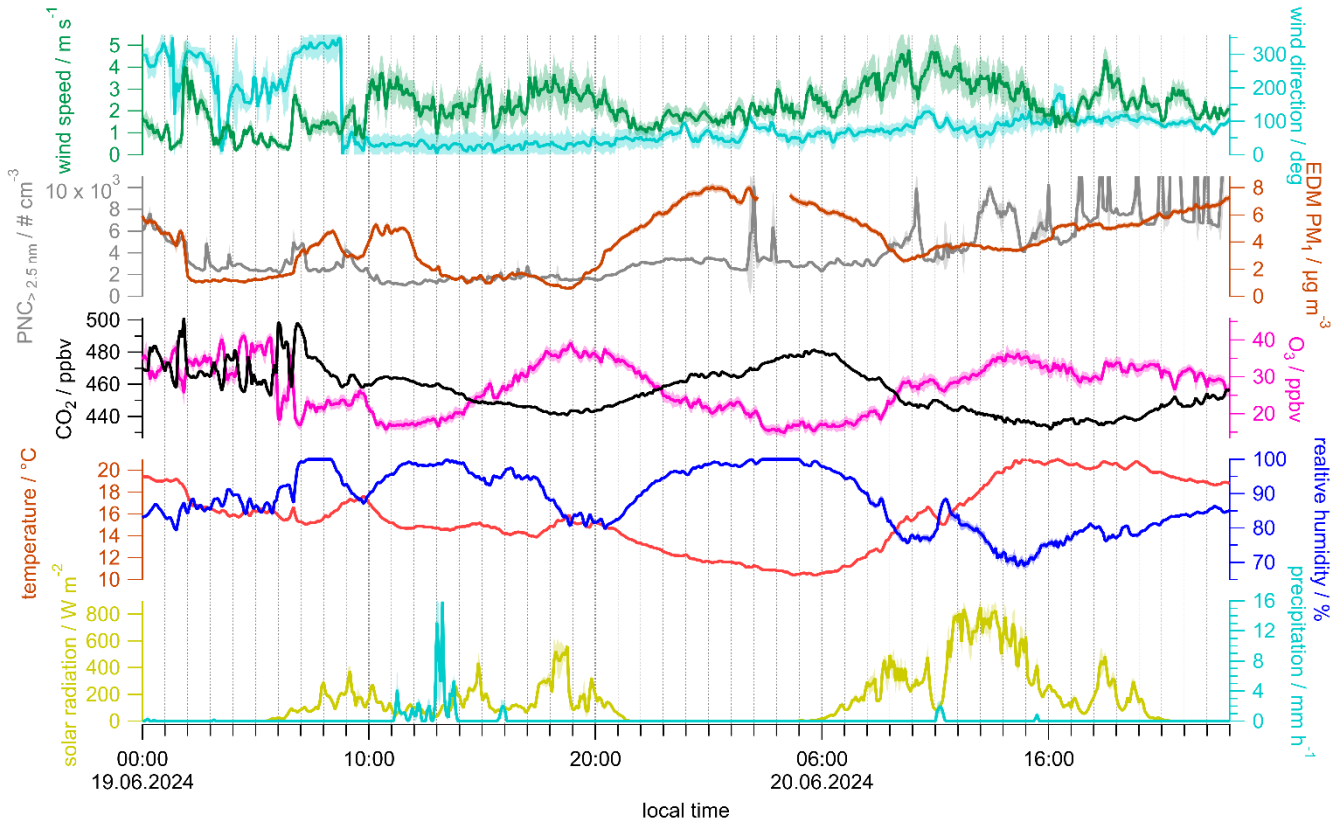

Figure S4: Ground-based measurements on June 19 to June 21, 2024 show low solar irradiation on June 19 and fog between 03:00 and 05:00 on June 20 that led to an increase of the measured PM_1 (dried, orange) and particle number concentration (grey), but a strong reduction of O_3 (pink), while air temperature (red), wind (green and turquoise) and CO_2 (black) appear unchanged.

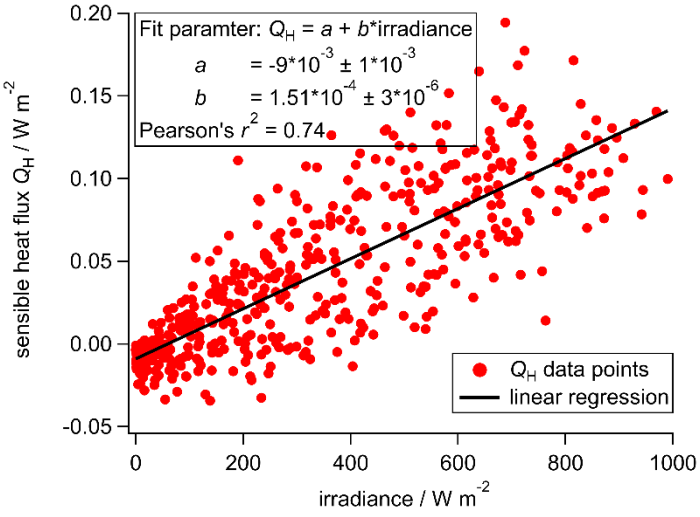

Figure S5: The sensible heat flux plotted versus solar irradiance during BISTUM24 show a good correlation (Pearson's $r^2 = 0.74$).

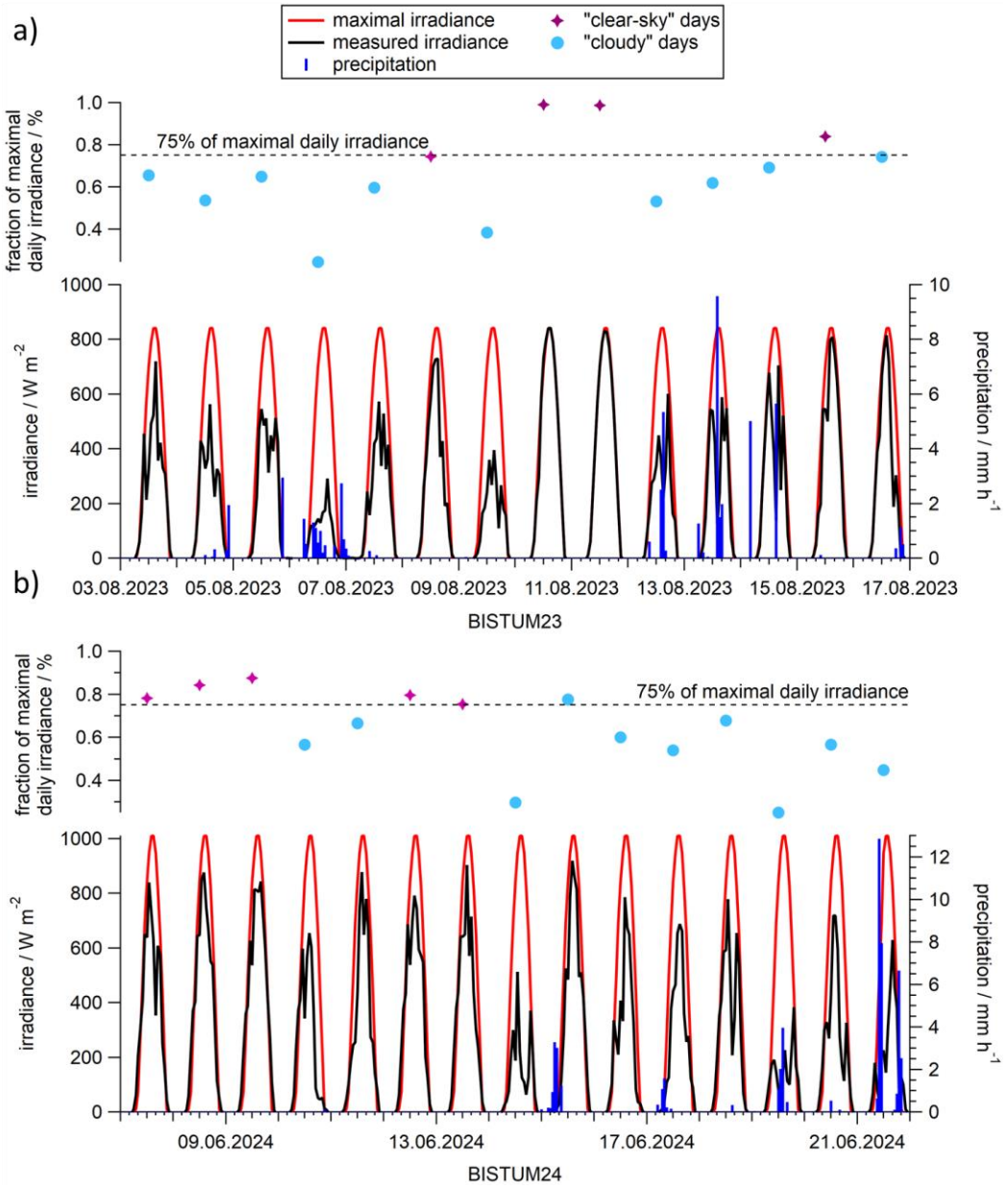

35 **Figure S6:** "Clear-sky" days (violet markers) and "cloudy" days (bluish markers) were classified by the criteria whether more or less than 75% of maximal daily possible irradiance (red traces) were measured (black traces) integrated throughout a day, respectively, and that precipitation (blue) was less/more than 5 mm day^{-1}. The classification of individual days is displayed for BISTUM23 (a) and BISTUM24 (b).

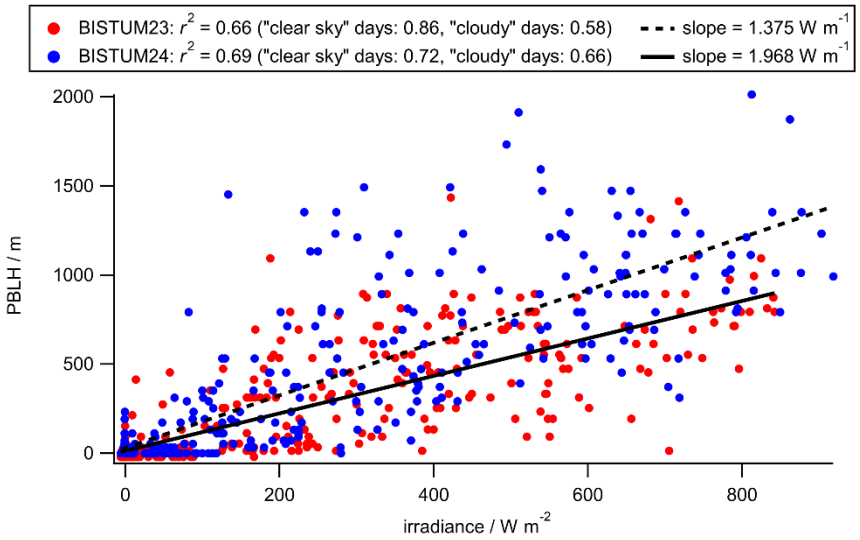

Figure S7: The modeled planetary boundary layer height (PBLH) versus the irradiance show a linear relationship for BISTUM23 (red) and BISTU24 (blue). The respective Pearson's correlation coefficients r^2 are higher for only "clear sky days compared to when solely "cloudy" days are considered.

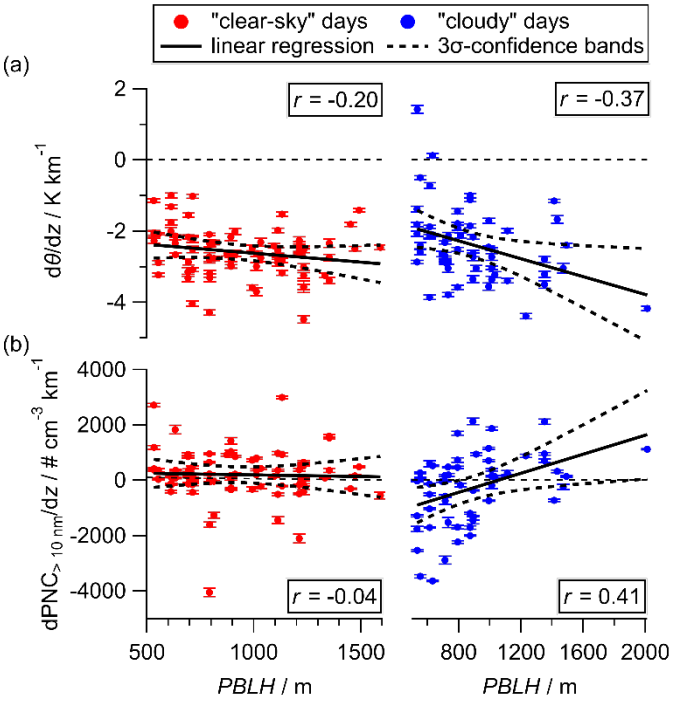

Figure S8: Gradients of the potential temperature θ (a) and the particle number concentration $PNC_{>10\ nm}$ (b) in the lowermost 500 m in a mixed PBL from both campaigns versus the non-logarithmic planetary boundary layer height (PBLH, in m). Linear regression and its 3σ-confidence bands are depicted in solid and dotted lines.

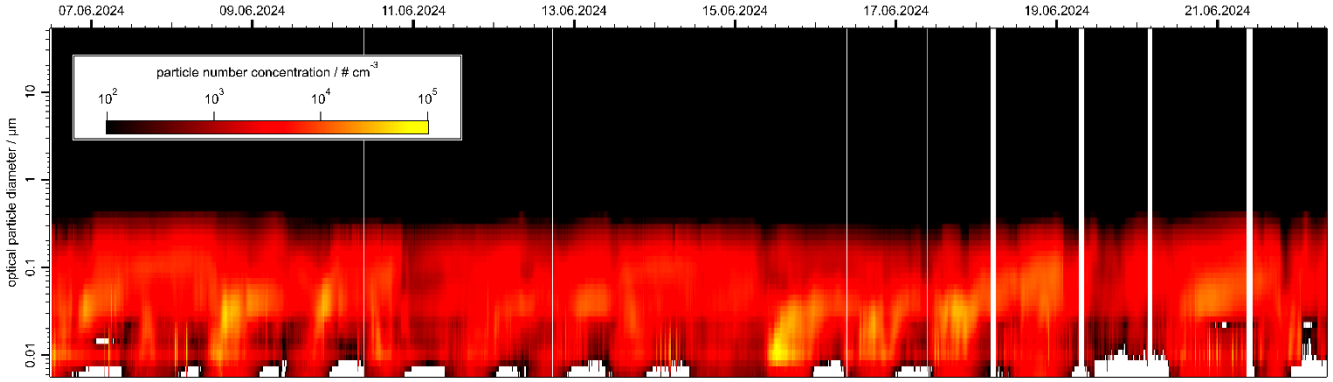

Figure S9: Throughout BISTUM24, the merged particle size distribution (described in Pikmann et al., 2024) shows new particle formation events almost daily. New particle formation is indicated by the growth of sub-10 nm particles after noon and is further described in Kulmala et al. (2004).

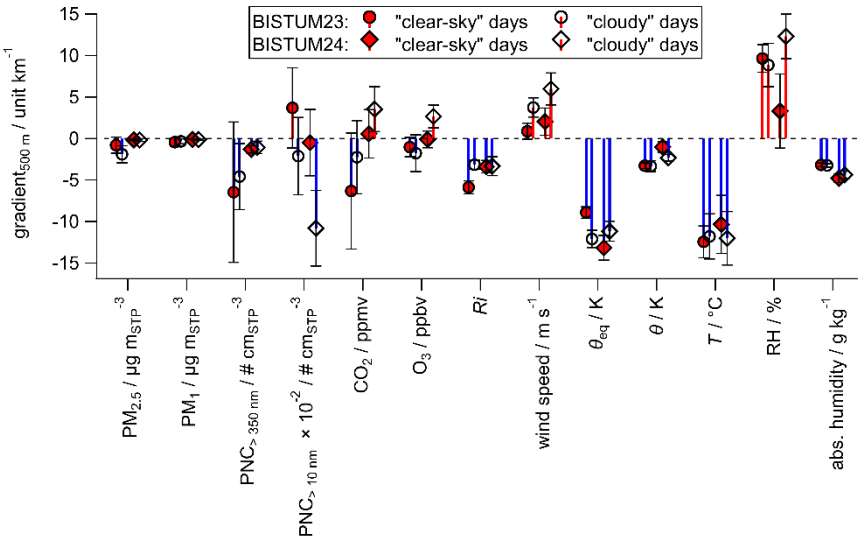

Figure S10: Vertical gradients in the lowermost 500 m in a mixed PBL for meteorological and trace matter variables during two campaigns (circles and diamonds) for "clear-sky" and "cloudy" days (red and white filled markers, respectively). Blue bars show negative, red bars positive gradients, and error bars represent the overall uncertainty, mainly due to day-to-day variability.

References

Drewnick, F., Böttger, T., von der Weiden-Reinmüller, S. L., Zorn, S. R., Klimach, T., Schneider, J., and Borrmann, S.: Design of a mobile aerosol research laboratory and data processing tools for effective stationary and mobile field measurements, Atmospheric Measurement Techniques, 5, 1443-1457, https://doi.org/10.5194/amt-5-1443-2012, 2012.

Kulmala, M., Vehkamäki, H., Petäjä, T., Dal Maso, M., Lauri, A., Kerminen, V. M., Birmili, W., and McMurry, P. H.: Formation and growth rates of ultrafine atmospheric particles: a review of observations, Journal of Aerosol Science, 35, 143-176, https://doi.org/10.1016/j.jaerosci.2003.10.003, 2004.

Moormann, L., Böttger, T., Schuhmann, P., Valero, L., Fachinger, F., and Drewnick, F.: The Flying Laboratory FLab: development and application of a UAS to measure aerosol particles and trace gases in the lower troposphere, Atmos. Meas. Tech., 18, 1441-1459, https://doi.org/10.5194/amt-18-1441-2025, 2025.

Pikmann, J., Drewnick, F., Fachinger, F., and Borrmann, S.: Particulate emissions from cooking: emission factors, emission dynamics, and mass spectrometric analysis for different cooking methods, Atmos. Chem. Phys., 24, 12295-12321, https://doi.org/10.5194/acp-24-12295-2024, 2024.